In situ probing of Pt/TiO_2 activity in low-temperature ammonia oxidation

Received 31st July 2020,
Accepted 04th November 2020

DOI: 10.1039/D0CY01533D

Lidiya S. Kibis,[a] Dmitry A. Svintsitskiy,[a] Andrey I. Stadnichenko,[a] Elena M. Slavinskaya,[a] Anatoly V. Romanenko,[a] Elizaveta A. Fedorova,[a] Olga A. Stonkus,[a] Valery A. Svetlichnyi,[b] Elena D. Fakhrutdinova,[b] Mykhailo Vorokhta,[c] Břetislav Šmíd,[c] Dmitry E. Doronkin,[d,e] Vasyl Marchuk,[d] Jan-Dierk Grunwaldt,*[d,e] and Andrei I. Boronin*[a]

The improvement of the low-temperature activity of the supported platinum catalysts in selective ammonia oxidation to nitrogen is still a challenging task. The recent developments in *in situ/operando* characterization techniques allows to bring new insight into the properties of the systems in correlation with their catalytic activity. In this work, near ambient pressure X-ray photoelectron spectroscopy (NAP-XPS) and *operando* X-ray absorption spectroscopy (XAS) techniques were applied to study Pt/TiO_2 catalysts in ammonia oxidation (NH_3+O_2 reaction). Several synthesis methods were used to obtain samples with different size of Pt particles, oxidation state of Pt, and morphology of the support. Metal platinum particles on titania prepared by pulsed laser ablation in liquids exhibited the highest activity at lower temperatures with the temperature of 50% conversion of NH_3 being 150°C. The low-temperature activity of the catalysts synthesized by impregnation can be improved by the reductive pretreatment. NAP-XPS and *operando* XANES data do not show formation of PtO_x surface layers or PtO/PtO_2 oxides during NH_3+O_2 reaction. Despite the differences in the oxidation state of platinum in the as-prepared catalysts, their treatment in the reaction mixture results in the formation of metallic platinum particles, which can serve as centers for stabilization of the adsorbed oxygen species. Stabilization of the bulk platinum oxide structures in the Pt/TiO_2 catalysts seems to be less favorable due to the metal-support interaction.

Introduction

Pt-containing catalysts are important components of the complex systems used for the exhausts gas aftertreatment.[1–4] Supported platinum systems are utilized in diesel vehicles, among others, as a part of ammonia slip catalysts responsible for NH_3 oxidation to molecular nitrogen.[5,6]

Both model platinum systems – single-crystals, foils, and gauzes,[7–12] as well as supported platinum catalysts,[13–20] have been studied in detail as catalysts for the ammonia oxidation reaction, mostly within the Ostwald process for nitric acid production. DFT calculations[21–25] and kinetic modeling[26–28] were performed to gain more insight into the mechanism. However, ways to improve the low-temperature activity (T<250°C) of the catalysts and the selectivity of the reaction towards N_2 formation (required for exhaust gas aftertreatment) are still under discussion. For supported Pt systems, activity and selectivity of the catalysts are influenced by many factors: the size of the platinum particles, Pt oxidation state, the structure and nature of the support, metal-support interactions, etc. Also, the state of the active component can change during the reaction process, which requires special experimental approaches to obtain relevant results. This makes it difficult to draw reliable conclusion on "structure" - "activity/selectivity" correlations.

The recent development of *in situ* and *operando* techniques opens new opportunities to get information about the systems under reaction conditions. *In situ* methods play a key role in studying reaction mechanisms and identifying the main factors affecting the activity and selectivity of the catalysts. Thus, *in situ* X-ray photoelectron spectroscopy (XPS) gives information about processes taking place on the surface of the catalysts during the reaction: the reaction intermediates formed on the surface can be identified; the change of the charge state of the active component can be analyzed. *In situ* XPS data for ammonia oxidation reaction on the surface of bulk platinum systems have already been reported.[10] The authors used stepped platinum surface which might to some extent simulate the structural heterogeneity of nanoparticles present in real powder catalysts. However, to obtain more relevant results, a further transition to the study of supported systems is necessary.

In this paper, we present a study of Pt/TiO_2 catalysts by *in situ/operando* methods in the ammonia oxidation reaction. The Pt/TiO_2 systems are less investigated for this reaction than the traditionally used Pt/Al_2O_3.[29,30] However, unlike the Pt/Al_2O_3 catalysts, for the Pt/TiO_2 system, there is a possibility of the metal-support interaction, which can influence the catalytic properties.[31–36] It was shown that the metal-support interaction can provide stabilization of the metal platinum particles.[31,33] Oxidation of the metal platinum particles with the formation of the oxide structures on the surface leads to deactivation of the catalysts of the ammonia oxidation reaction.[13,19,37] Therefore, stabilization of metallic Pt species might be beneficial for the NH_3+O_2 catalytic process. As

[a] Boreskov Institute of Catalysis, pr. Lavrentieva 5, 630090, Novosibirsk, Russia. E-mail: boronin@catalysis.ru
[b] Tomsk State University, pr. Lenina 36, 634050, Tomsk, Russia
[c] Charles University, Department of Surface and Plasma Science, Faculty of Mathematics and Physics, V Holešovičkách 2, 180 00, Prague 8, Czech Republic
[d] Institute for Chemical Technology and Polymer Chemistry (ITCP), Karlsruhe Institute of Technology, Engesserstr. 20, 76131, Karlsruhe, Germany E-mail: grunwaldt@kit.edu
[e] Institute of Catalysis Research and Technology (IKFT), Karlsruhe Institute of Technology, Hermann-von-Helmholtz-Platz 1, 76344, Eggenstein-Leopoldshafen, Germany

† Electronic Supplementary Information (ESI) available: Fig.S1-S11. See DOI: 10.1039/D0CY01533D

potential catalysts for the selective NH_3 oxidation at low temperature, the Pt/TiO_2 systems should be investigated in detail using the modern physicochemical methods.

Two techniques for the synthesis of Pt/TiO_2 catalysts were applied in this work. Apart from the traditional impregnation technique, pulsed laser ablation in liquids (LAL) was used for the synthesis of the catalysts. The LAL method leads to the formation of the dispersed particles with a defective, distorted structure.[38–41] As the defects of the TiO_2 support might stimulate the metal-support interaction,[42–44] the LAL can be a promising method for the preparation of the Pt/TiO_2 catalysts active in the ammonia oxidation reaction. Previously, it was shown that the composites prepared by LAL are active in CO oxidation reaction,[38,39] low-temperature ammonia oxidation,[45] phenol photodegradation process under visible light.[41]

The supported Pt/TiO_2 catalysts were studied using NAP-XPS and *operando* XAS – powerful complementary tools for the investigation of the catalysts under working conditions. The application of these methods provided insights into the evolution of the surface and bulk Pt particle structure under NH_3+O_2 conditions showing that the metal platinum particles do not undergo significant oxidation under the reaction conditions, regardless of the preparation method.

Experimental

Samples preparation

Two approaches were used for the synthesis of Pt/TiO_2 samples. The first was the incipient wetness impregnation of the commercial TiO_2 support (AEROXIDE P25, Evonik) with a solution of platinum nitrate $Pt(NO_3)_x$ (17.87 wt.%, KZCM). The resulted sample was dried at room temperature (for 16h) with further increase of the temperature to 60°C (heating for 1h) and 120°C (heating for 2h). The dried catalyst was calcined in air at 400°C for 4h. The platinum content in the sample was 2 wt.%. This sample is denoted by Pt/TiO_2-IMP in the text.

The second method for the synthesis of the catalysts was pulsed laser ablation in liquids. The detailed description of the preparation of the composite catalysts by the LAL is given in [38,39]. Briefly, the Pt and TiO_x dispersions were obtained separately by ablation of platinum and titanium metal plates in liquids. The ablation of the targets was carried out by focused radiation of a Nd: YAG laser (1064 nm, 7 ns, 150 mJ imp., 20 Hz). Based on the earlier study,[39] an ethanol solution (96.3 vol.%) and distilled water were taken as solvents to obtain platinum and TiO_x dispersions, respectively. The concentration of the components in the resulting dispersions was determined by the loss of the mass of the corresponding target. The resulting solutions were mixed in such a proportion so as to obtain 2 wt.% of platinum in the catalyst. The Pt and TiO_x dispersions were mixed using a magnetic stirrer at room temperature and dried in air at 60°C. The air-dried powder was calcined in air at 400°C for 4h. The LAL-prepared sample is denoted in the text by Pt/TiO_2-LAL.

Physicochemical characterization

To characterize the structure of the catalysts X-ray diffraction (XRD) and transmission electron microscopy (TEM) were used. The XRD data for the catalysts were obtained on a Bruker D8 instrument (Germany) using Cu *Kα* radiation in a 2θ range 15°<2θ<90° (step size 0.05°, 5 s per step). Diffraction intensities were measured with the LynxEye position sensitive detector. For crystalline phase analysis, the ICDD PDF-2 powder database was used. The refinement of the structure and the profile analysis were carried out with the TOPAS software package (Bruker, Germany).[46]

TEM experiments were performed on a JEM-2200FS electron microscope (JEOL Ltd., Japan) at the "VTAN" resource center of Novosibirsk State University, Russia. To collect the high-resolution (HRTEM) and HAADF-STEM images with a spatial resolution of 1 Å an accelerating voltage of 200 kV was applied. TEM data were analyzed using "ImageJ" software[47] to determine the particle size distribution. For TEM experiments samples were deposited on 3 mm copper grids coated with a carbon film by dispersing in ethanol and sputtering the dispersion on the grids.

The specific surface area of the samples (S_{BET}) was determined by the standard Brunauer–Emmett–Teller method using the low-temperature adsorption isotherms of N_2 collected at an ASAP-2400 setup (Micromeritics Instrument. Corp., Norcross, GA, USA).

Analysis of the samples by X-ray photoelectron spectroscopy (XPS) under UHV ($p\sim10^{-8}$ mbar) conditions (*ex situ* XPS experiments) was performed using an ES-300 spectrometer (KRATOS Analytical). To record the spectra a non-monochromatic Mg *Kα* source (hν = 1253.6 eV) was employed.

In situ XPS data were collected at a near ambient pressure XPS setup (SPECS Surface Nano Analysis, GmbH Germany) at the Charles University (Prague, Czech Republic). A monochromatic Al *Kα* source (hν = 1486.6 eV) was used to collect XPS spectra. The powder catalysts were pressed to pellets and fixed on the sample holder using spot welding of Ta foil stripes. The sample holder contained a K-type thermocouple welded near the sample pellet for temperature control. Heating was performed by the electron bombardment at the back of the sample stage, which was in thermal contact with the sample holder while mounted on the NAP manipulator. XPS analysis of the samples before their exposure to the reaction mixture was performed at room temperature (RT) in Ar flow (p(Ar)~1 mbar) to prevent the surface charging. The *in situ* experiments were performed by stepwise heating the samples in the NH_3+O_2 reaction mixture (NH_3:O_2 ratio of 1:40 and total pressure p_Σ~1.4 mbar) from 50°C to 400°C with simultaneous acquisition of XPS data. XPS spectra were collected after heating the samples to a certain temperature and stabilization in the reaction mixture for 20 min. XPS experiments were complemented with simultaneous analysis of the gas mixture by mass spectrometry (Prisma Pro, Pfeiffer Vacuum, Germany) to follow the change of concentrations of the reagents (NH_3, O_2) and products (H_2O, N_2O, N_2, NO_x) with temperature increase.

The spectra energy calibration was done using a $Ti2p_{3/2}$ line as an internal standard with a binding energy value $E_b(Ti2p_{3/2})$=458.6 eV for TiO_2. Such a calibration procedure gave E_b(C1s)=284.7 eV for the residual amorphous carbon present on the surface. The Pt4f/Ti2p ratio was calculated based on the area of the corresponding spectral lines. The Shirley background was subtracted before processing the spectra. Ti2p, O1s, C1s, and N1s spectra were fitted with a combination of the Gaussian and Lorentzian functions The Pt4f spectra fitting was performed using a combination of the Gaussian and Lorentzian functions for oxidized components, while Doniach–Šunjić function was used to describe the asymmetry of metallic Pt^0 doublet. Also, Pt4f spectra fitting was performed with consideration of the FWHM (full width at half maximum) values of the corresponding Ti2p lines. The XPS-Calc program[38,39] was used for processing the XPS data.

Ex situ and *operando* X-ray absorption near edge structure (XANES) spectra at Pt L_3 absorption edge were recorded at the P65 beamline of the PETRA III synchrotron radiation source (DESY, Hamburg, Germany) in transmission mode. Energy of the X-rays was selected using a Si(111) double crystal monochromator and higher harmonics were rejected by a pair of Si mirrors. Beam size was selected by slits as 0.2 (vert.) × 1.0 (hor.) mm^2. Catalyst samples were measured as 100-200 µm sieved powders packed in quartz capillaries (o.d. = 1.5 mm, 0.02 mm wall thickness) heated by a hot air blower. The catalyst bed length was approx. 5 mm and the X-ray beam was probing part near inlet of the catalyst bed. The gas mixture contained 880 ppm NH_3, 10 vol.% O_2, and 10 vol.% N_2 in He with a flow of 70 ml/min. Outlet gas composition was analyzed by an MKS Multigas 2030 FTIR analyzer. The spectra were corrected for the energy shift using a spectrum of Pt foil measured simultaneously and then normalized using the Athena program from the IFFEFIT software package.[48] The average oxidation state of Pt was determined by linear combination analysis (LCA) of the XANES data in Athena[48] with Pt foil and PtO_2 reference spectra in the energy range between 11550 and 11600 eV. For the analysis of extended X-ray absorption fine structure (EXAFS), the spectra were background-subtracted, k^2-weighted, multiplied by a Hanning window with sill size of 1 $Å^{-1}$, and Fourier-transformed in the k-range 2.5-11.0 $Å^{-1}$. The amplitude reduction factor S_0^2=0.74 was obtained by fitting the Pt foil and the PtO_2 (Alfa Aesar, 99.95%) reference spectra to structural models as reported in the *Inorganic Crystal Structure Database (ICSD, CCs = 64923 and 4415).* The fits were performed on k^1, k^2, and k^3-weighted using Artemis[48] by a least square method in R-space between 1.0 and 3.0 Å. Coordination numbers, interatomic distances, energy shift (δE_0) and mean square deviation of interatomic distances (σ^2) were refined during the fitting. The absolute misfit between theory and experiment was expressed by ρ.

Catalytic experiments

The catalytic properties of the Pt/TiO_2 samples were studied in the temperature-programmed reaction of ammonia oxidation (TPR-NH_3+O_2). The experiments were performed in a plug flow quartz reactor. 0.145 g of the catalyst was analyzed in the catalytic experiments. Heating of the samples in the NH_3+O_2 mixture was performed from room temperature to 400°C at a rate of 10°C/min. The reaction mixture containing 0.1 vol.% NH_3, 4.0 vol.% O_2 (balance He) was fed at a flow of 500 ml/min. Before TPR-NH_3+O_2 experiments, Pt/TiO_2-LAL and Pt/TiO_2-IMP samples were heated in 20%O_2/He flow at 400°C for 2 h to remove the surface admixtures. A gas-phase FTIR spectrometer (I1801, MIDAC corp., USA) was used to measure concentrations of NH_3, N_2O, NO, NO_2, while O_2 and N_2 concentrations were analyzed using a gas chromatograph (Crystal 2000M, CHROMATEC, Russia). Conversion (in %) of ammonia was calculated as $X_{NH3}=(1-C_{NH3}^{out}/C_{NH3}^{in})\cdot 100$, where C_{NH3}^{in} and C_{NH3}^{out} are the inlet and outlet NH_3 concentrations, respectively. Selectivity (in %) to the reaction products (N_2, N_2O, NO, or NO_2) was calculated as $S_i=(n_i/\Sigma n_i)\cdot 100$, where n_i – the concentration of the corresponding product.

Results and discussion

Structural characterization of Pt/TiO_2 samples

Fig.1 shows the X-ray diffraction patterns for Pt/TiO_2-LAL (purple line (1)) and Pt/TiO_2-IMP (green line (2)) samples. For obtained XRD patterns, a full profile Rietveld refinement was performed. The XRD profile Rietveld modeling for the samples are given in ESI file (Fig.S1). The Pt/TiO_2-LAL sample contains an X-ray amorphous phase as well as the crystalline phases attributed to metallic Pt (ICDD PDF-2 # 04-0802) and anatase structure of TiO_2 (ICDD PDF-2 # 21-1272). The calculated diffraction curve poorly describes the experimental pattern in the region of the anatase reflections (see Fig.S1), which

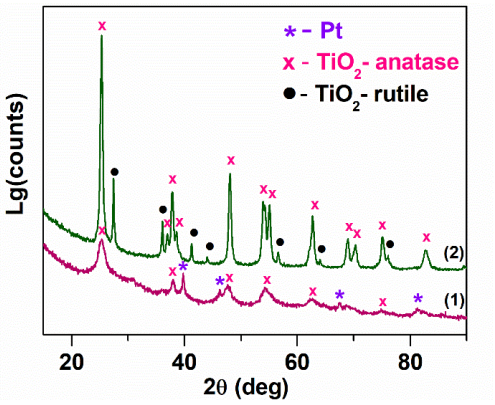

Fig.1. X-ray diffraction patterns for (1) Pt/TiO_2-LAL, (2) Pt/TiO_2-IMP.

Table 1. Morphology and structural characteristics of the catalysts.

	S_{BET}, m^2/g	TiO_2-anatase				TiO_2-rutile			
		a, Å	*c*, Å	*D*, nm	W, wt.%	*a*, Å	*c*, Å	*D*, nm	W, wt.%
Pt/TiO_2-LAL	152	3.804(3)	9.47 (1)	4.7 (3)	100	-	-	-	-
Pt/TiO_2-IMP	63	3.786(1)	9.508(1)	18.8 (3)	84.1 (6)	4.595(1)	2.960(1)	29 (2)	15.9 (6)

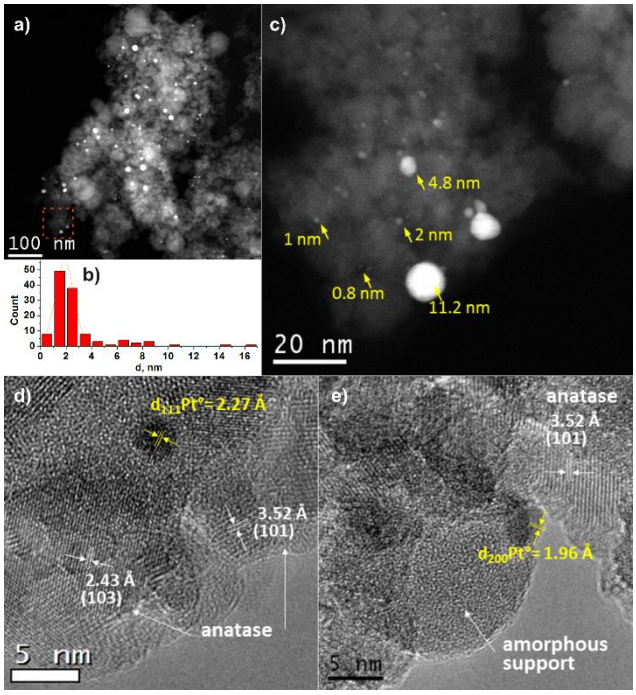

Fig.2. STEM and HRTEM study of the Pt/TiO_2-LAL sample: (a) HAADF-STEM data, (b) Pt particle size distribution, (c) HAADF-STEM data of the area marked in (a) with red square, (d,e) HRTEM data of selected regions.

suggests that the anatase phase might be defective. The structural characteristics of the TiO_2 phases (lattice parameters (*a,c*), the average crystallite size (*D*)) calculated from XRD data are given in Table 1. There is a difference between the values of the TiO_2-anatase lattice parameters for the Pt/TiO_2-LAL sample and the data reported for the single crystal anatase TiO_2 (*a*=3.784 Å, *c*=9.515 Å).[49] Ballirano et al.[50] observed the modified lattice parameters (*a*=3.784 Å, *c*=9.500 Å) for the nanosized TiO_2-anatase particles (*D*~21 nm). For the Pt/TiO_2-LAL sample, the calculated average crystallite size is ~5 nm. Thus, the change of the lattice parameters of the anatase phase might be related to the small size and defective structure of the TiO_2 crystallites. Contribution from the metallic Pt in the Pt/TiO_2-LAL sample was refined with the introduction of two phases corresponding to large (*D*~25 nm) and small particles (*D*~2 nm).

The X-ray diffraction pattern of the Pt/TiO_2-IMP sample can be described with a mixture of anatase (ICDD PDF-2 # 21-1272) and rutile (ICDD PDF-2 # 21-1276) phases. The amount of the anatase phase is greater than the rutile phase (see Table 1). The average crystallite sizes of anatase and rutile phases are ~19 nm and ~30 nm, respectively. The lattice parameters of the TiO_2 phases are similar to those reported for the nanosized TiO_2.[50] Platinum-containing phases were not detected by the XRD method allowing us to propose the presence of the highly dispersed Pt species in the Pt/TiO_2-IMP sample.

The smaller size of the TiO_2 crystallites in the Pt/TiO_2-LAL sample results in a higher value of the surface area (S_{BET}) in comparison with the Pt/TiO_2-IMP sample (see Table 1).

Fig.2 shows TEM data for the Pt/TiO_2-LAL sample. Most of the TiO_2 particles are 5-10 nm in size, but larger particles from 10 to 200 nm in diameter are also observed. Both the crystalline phase of anatase (Fig.2d) and amorphous TiO_x particles (Fig.2e) can be identified using HRTEM.

Platinum nanoparticles in the Pt/TiO_2-LAL sample have a spherical-like shape. Their distribution over the support is

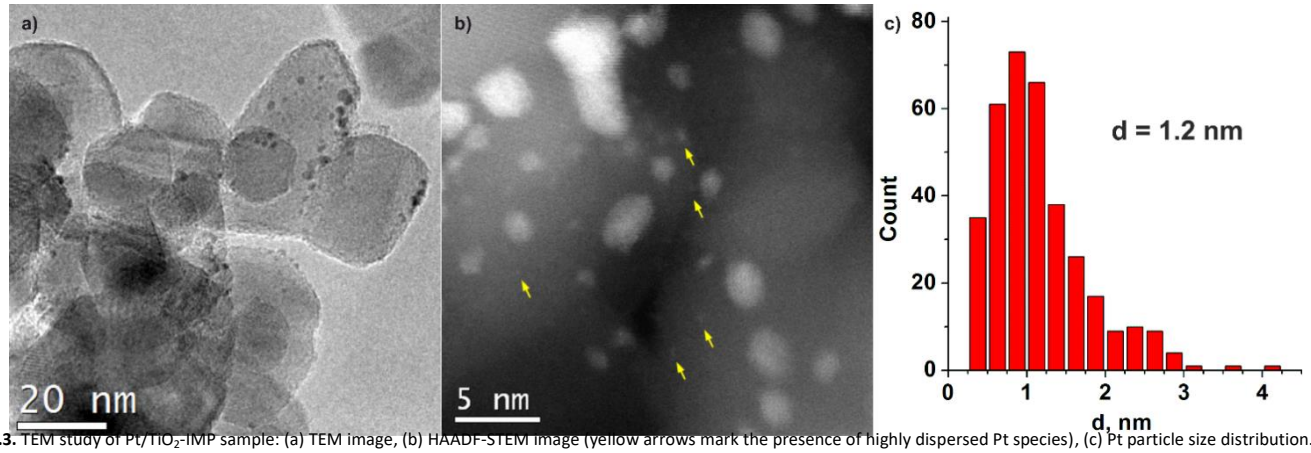

Fig.3. TEM study of Pt/TiO_2-IMP sample: (a) TEM image, (b) HAADF-STEM image (yellow arrows mark the presence of highly dispersed Pt species), (c) Pt particle size distribution.

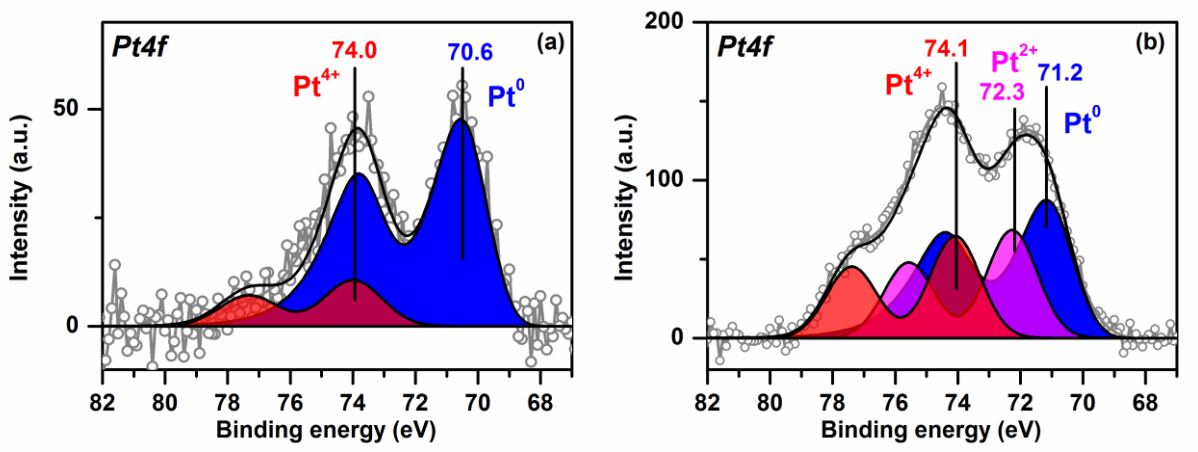

Fig.4. Pt4f XP spectra for (a) Pt/TiO_2-LAL, (b) Pt/TiO_2-IMP samples.

uniform. Most of the platinum particles have a size of 1-3 nm (Fig.2b). However, there are some larger particles with a size of 10-20 nm. The results are in a good agreement with the XRD data.

TEM data for the Pt/TiO_2-IMP sample are given in Fig.3. The size of the TiO_2 particles varies from 10 to 40 nm. The Pt nanoparticles have a spherical-like shape (Fig.3a). The average size of platinum particles is 1.2 nm (Fig.3c). Also, highly dispersed platinum particles less than 1 nm in size (marked with yellow arrows in Fig.3b) can be well detected due to the high contrast of platinum on the TiO_2 surface in the dark-field images (Z-contrast).

XPS analysis of the Pt/TiO_2 samples in UHV

Fig.4 shows the Pt4f X-ray photoelectron (XP) spectra of the Pt/TiO_2 samples fitted to the individual components. The Ti2p and O1s spectra of the samples are given in ESI, Fig.S2. For Pt/TiO_2-LAL sample the main Pt4f doublet has a $E_b(Pt4f_{7/2})$ value 70.6 eV (Fig.4a). The $E_b(Pt4f_{7/2})$ value typical for bulk metal Pt^0 surfaces (foils, single-crystals etc.) is usually considered to be 71.0-71.2 eV.[51–53] It cannot be excluded that the interaction of the Pt^0 nanoparticles with the TiO_2 support results in a slight decrease of the observed $E_b(Pt4f_{7/2})$ value for the Pt/TiO_2-LAL sample. Metal-support interaction is known for the supported catalytic systems.[42,44,54–57] It can cause a change in the electronic state of the active component and the support, structure, and morphology of the catalyst. For the Pt-TiO_2 systems, metal-support interaction is most frequently discussed in terms of the charge transfer from TiO_2 to the small Pt particles[32,55,58] with accumulation of the charge at the Pt-TiO_2 interface[55] or encapsulation of the platinum particles by the support.[32,34,54,59] Metal-support interaction is usually observed when samples are heated in a reductive atmosphere. ~~In~~ Under these conditions, the reduced, defective $TiO_{2-\delta}$ structures might be formed facilitating the interaction with Pt particles.[42–44] In our case, the LAL method leads to the formation of defective, amorphous structures of titanium oxide, hence, a metal-support interaction might occur. The accumulation of the charge at the Pt^0-TiO_2 interface can cause the inhomogeneous charging of the sample surface, thus resulting the observed negative shift of Pt^0 peaks.

A $Pt4f_{7/2}$ peak with a lower intensity at ~74.0 eV (Fig.4a) can be related to oxidized Pt^{4+} species.[51,60] It is known that small platinum particles can be easily oxidized with the formation of PtO_x structures.[61–65] TEM data for the Pt/TiO_2-LAL sample show the presence of a certain amount of the highly dispersed platinum species. We can propose the highly dispersed Pt species are in Pt^{4+} oxidation state.

The Pt4f region for the Pt/TiO_2-IMP catalyst reveals three platinum states with the $E_b(Pt4f_{7/2})$ values of 71.2, 72.3 and 74.1 eV (Fig.4b). The first state might be attributed to the metallic platinum species.[51,53,60] The second and third states of platinum can be related to Pt^{2+} and Pt^{4+} species, respectively.[51,53,60] The stoichiometry of the PtO_x species formed by interaction of small platinum particles with oxygen depends on the particle size. According to Wang et. al.,[66] the x value changes from 1 to 2 when particle size decreases below 2 nm. Since we have a distribution of the size of the Pt particles, it can be proposed that the smallest platinum particles oxidize to PtO_2, while the larger particles give PtO species. The formation of a PtO oxide layer covering the surface of the metal platinum particles is also possible. Thus, the observed Pt^{2+} oxidized species can be present as a PtO layer on the surface of Pt^0 particles and/or as oxidized PtO particles. Zhang et al. also observed peaks at 71.2 eV and 72.3 eV for a Pt-TiO_2 film calcined at 400°C.[67] The authors proposed oxidation of Pt^0 sites to Pt^{2+} species which substitute Ti^{4+} ions in TiO_2 lattice. Hence, the stabilization of the Pt^{2+} species due to the interaction with the TiO_2 lattice cannot be ruled out.

The contribution of the oxidized platinum species to the Pt4f spectrum for Pt/TiO_2-IMP sample is higher than in the case of the Pt/TiO_2-LAL sample. Such a result is in a good agreement with the TEM data which show higher amount of the highly dispersed platinum species in the Pt/TiO_2-IMP sample.

The ratio of the Pt4f and Ti2p line intensities (Pt4f/Ti2p) in the Pt/TiO_2-LAL is significantly lower (about 3.5 times) than for the Pt/TiO_2-IMP. This can be explained by the presence in the Pt/TiO_2-LAL sample a certain amount of the large platinum

particles which results in low intensity of the platinum signal. A partial encapsulation of the platinum particles by a TiO_x layer is also possible. Furthermore, the S_{BET} of the Pt/TiO_2-LAL sample is almost 2.5 times higher than the one of the Pt/TiO_2-IMP

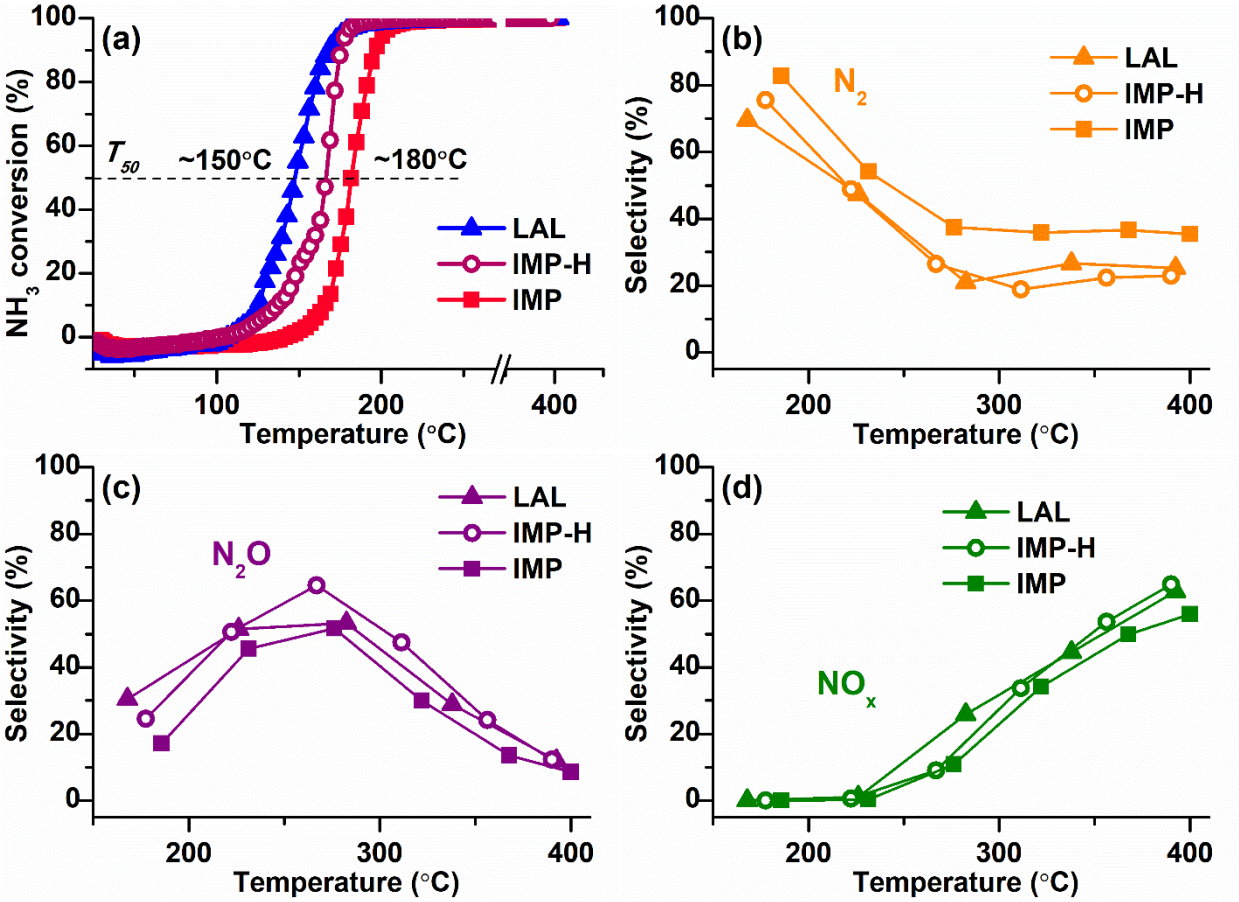

Fig. 5. TPR-NH_3+O_2 data for Pt/TiO_2 catalysts: (a) NH_3 conversion; products selectivity: (b) N_2, (c) N_2O, (d) NO_x. Sample Pt/TiO_2-LAL marked as triangles, Pt/TiO_2-IMP as squares, and Pt/TiO_2-IMP-H as circles. The reaction mixture: 0.1 vol.% NH_3 and 4.0 vol.% O_2 (balance He).

sample (see Table 1). This can lead to a higher intensity of the titanium signal due to larger surface.

To sum up, the *ex situ* characterization shows that the sample prepared using the LAL technique comprises mostly metallic platinum nanoparticles in contact with TiO_2. The Pt/TiO_2-IMP sample shows more dispersed and oxidized platinum particles.

Catalytic activity of the Pt/TiO_2 samples in NH_3+O_2 reaction

The activity of the samples in ammonia oxidation was studied using the temperature-programmed reaction NH_3+O_2 (TPR-NH_3+O_2). Data on the ammonia conversion and the selectivity to the reaction products as function of the temperature are given in Fig.5.

All samples show low-temperature activity reaching 100% conversion of ammonia at T<200°C. Comparison of the NH_3 conversion curves shows that the Pt/TiO_2-LAL sample is more active at low temperatures. The temperature of the 50% ammonia conversion (T_{50}) is ~150°C, while for the Pt/TiO_2-IMP sample the T_{50} value is ~180°C. Metallic platinum is proposed to be more active in the oxidation of ammonia in O_2 excess.[68,69] Therefore, higher low-temperature activity observed for the Pt/TiO_2-LAL sample can be attributed to the presence of higher amount of the metallic platinum particles.

To confirm this assumption, the Pt/TiO_2-IMP sample was reduced in 20%H_2/He flow at 250°C for 2 h in a catalytic reactor directly before the catalytic experiments (the reduced sample is denoted by Pt/TiO_2-IMP-H). This procedure should lead to an increase of the amount of the reduced platinum forms, and, accordingly, contribute to the improvement of the low-temperature activity. Indeed, one can see a decrease of T_{50} value (Fig.5a, the IMP-H curve) for the Pt/TiO_2-IMP-H sample in comparison with the initial Pt/TiO_2-IMP catalyst.

The selectivity to the reaction products is similar for all samples. In the temperature range up to 250°C, the main products are molecular nitrogen and N_2O. The maximum selectivity of N_2 is observed in the region of NH_3 conversion below 100% (T<200°C). At higher temperature the contribution of nitrogen oxides becomes more significant: N_2O at lower temperatures, and NO and NO_2 oxides at temperatures above 320-350°C. Such temperature-dependent product distribution is typical for bulk Pt structures[8,10] as well as platinum particles stabilized on oxide supports.[15,69,70]

Thus, although all samples show activity in the NH_3+O_2 reaction at T<200°C, NH_3 conversion for the Pt/TiO_2-LAL and Pt/TiO_2-IMP-H samples is observed at lower temperatures. To follow the evolution of the oxidation/charge state of Pt during the catalytic reaction the samples were analyzed by NAP-XPS.

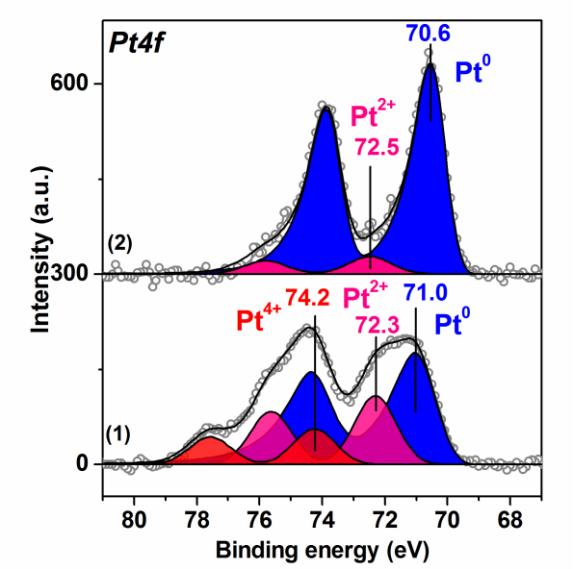

Fig.6. Curve-fitted *in situ* Pt4f XP spectra of (1) Pt/TiO_2-IMP and (2) Pt/TiO_2-IMP-H samples acquired in Ar (p(Ar)~1 mbar, RT).

NAP-XPS study of the Pt/TiO_2 samples

Fig.6 presents the Pt4f spectra fitted into the individual components for the Pt/TiO_2-IMP and the Pt/TiO_2-IMP-H samples collected at a NAP-XPS setup before exposure to the reaction mixture. The Pt/TiO_2-IMP-H sample was in this case prepared directly in the chamber of the NAP-XPS setup by reduction of the Pt/TiO_2-IMP in H_2 flow at 350°C for 2 h (p(H_2)~1 mbar). Ti2p and O1s spectra for Pt/TiO_2-IMP and Pt/TiO_2-IMP-H samples are given in ESI, Fig.S3.

Similar to the *ex situ* XPS data, the *in situ* Pt4f spectrum of the Pt/TiO_2-IMP sample shows three doublets with maxima of the $Pt4f_{7/2}$ peaks at binding energies ($E_b(Pt4f_{7/2})$) = 71.0 eV, 72.3 eV, and 74.2 eV. These doublets can be related to the Pt^0, Pt^{2+} and Pt^{4+} platinum species, respectively.[51,53,60]

Treatment of the Pt/TiO_2-IMP sample in H_2 flow results in reduction of Pt^{2+} and Pt^{4+} species. The Pt4f spectrum of the Pt/TiO_2-IMP-H sample (Fig.6 curve (2)) shows the main peak of the reduced Pt species at 70.6 eV. Heating of Pt/TiO_2 in a reductive atmosphere is known to promote the metal-support interaction.[42–44] We do not observe a noticeable change in the Pt4f/Ti2p intensity ratio upon sample heating in H_2, which suggests that the encapsulation of the platinum particles by the titania does not take place. Nevertheless, the charge transfer ~~from~~ between the support and the platinum particles might take place influencing the $E_b(Pt4f_{7/2})$ value. It can be assumed that the reductive treatment results in the formation of the defects on the surface of titania, which promotes the Pt-TiO_2 interaction. Unfortunately, due to the morphology of the supported powder catalysts and the rather low concentration of the active component, we could not detect any noticeable changes in the Ti2p spectra which might give information on the possible appearance of Ti^{3+} species due to metal-support interaction (see ESI, Fig.S3).

The state of platinum in the Pt/TiO_2-IMP-H sample is similar to the Pt/TiO_2-LAL catalyst (see Fig.4a). Pt4f spectra for both catalysts show the main Pt state with the $E_b(Pt4f_{7/2})$~70.6 eV, indicating a similar nature of active sites in these catalysts, namely: Pt^0 species in contact with TiO_2 surface. This is also confirmed by similar catalytic properties of these samples.

The Pt/TiO_2-IMP and Pt/TiO_2-IMP-H samples were heated in the NH_3+O_2 mixture with simultaneous collection of the NAP-XPS data. The change of the concentrations of the reagents and products with the increase of the reaction temperature was monitored with a mass-spectrometer. MS-data are given in ESI (Fig.S4). Both samples under given reaction conditions showed similar MS results. Conversion of NH_3 was observed at T>175°C. At temperature below 225°C, the main products were N_2 and N_2O, while at T~225°C partial pressure of NO increased and became predominant at 400°C. These results are in a good agreement with data of the catalytic experiments performed in a plug flow reactor (see Fig.5).

Fig.7 shows the evolution of the Pt4f XP spectra collected *in situ* during heating the Pt/TiO_2-IMP (Fig.7a) and Pt/TiO_2-IMP-H (Fig.7b) samples in the NH_3+O_2 mixture. Treatment of the Pt/TiO_2-IMP sample in the reaction mixture results in a slight increase of the $E_b(Pt4f_{7/2})$ value of the peak related to Pt^0 species. The conductivity of the sample surface might slightly change during the reaction due to the removal or accumulation of O-containing surface groups. Thus, the shift of the Pt^0 peaks can be caused by the variation of the charge over the sample surface.

Also, interaction of the platinum particles with oxygen can be the reason for the slight increase of the $E_b(Pt4f_{7/2})$ value. Different oxygen species can be formed on the Pt surface: adsorbed oxygen,[8,10,66,71] subsurface oxygen[72] or platinum oxide-like structures.[73–76] The conditions under which various surface oxide structures occur were studied in detail for Pt single-crystals,[73–75,77–79] foils, and nanoparticles.[60,72,80–83]

For surface and bulk platinum oxides, the binding energy of the $Pt4f_{7/2}$ peak is usually considered to be more than 72.0 eV.[73–76] Since we do not observe a strong shift of the Pt4f line (the binding energy does not exceed 71.4 eV), the formation of fully oxidized PtO_x layers or bulk oxides seems unlikely. Smirnov et al.[72,80] showed that dissolution of oxygen in platinum leads to an increase in the E_b value of the platinum line, while its metal nature is preserved. However, they also observed quite significant shifts of the Pt4f line (~1 eV) for small Pt particles (d~1-2.5 nm).[80]

Gland et al.[7] observed adsorption of oxygen atoms on edge sites of the stepped Pt single-crystal surface under ammonia oxidation reaction. Gunter et al.[10] detected in their study by *in situ* XPS of ammonia oxidation over a Pt(533) surface the formation of a 1D platinum oxide phase. Imbihl et al.[11] also showed that OH_{ad} as well as O_{ad} species should be considered during ammonia oxidation. Based on this, we can propose that the $E_b(Pt4f_{7/2})$ shift observed in our work might be caused by ~~is~~

the formation of adsorbed oxygen species (O_{ad} and/or OH_{ad}) on the Pt^0 surface or at the Pt^0-TiO_2 boundary. Unfortunately, analysis of the O1s spectra of the samples (see ESI, Fig.S5) does not allow to reliably detect signals related to the oxygen species adsorbed on the platinum surface due to low concentration of Pt in the samples, high intensity of the titania oxygen, and variety of the oxygen-containing species adsorbed on the sample surface. The increase of the $E_b(Pt4f_{7/2})$ value of the peaks related to the oxidized Pt^{2+} and Pt^{4+} species can be explained by the formation of the $Pt(OH)_x$ structures[51,84] due to

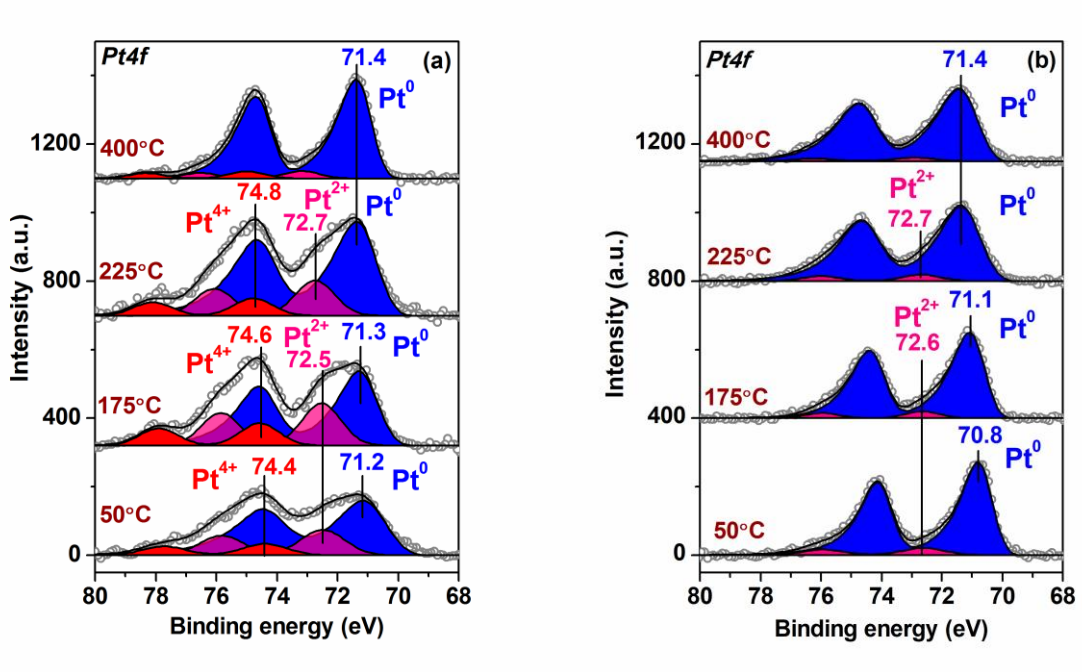

Fig.7. Curve-fitted *in situ* Pt4f XP spectra of (a) Pt/TiO_2-IMP and (b) Pt/TiO_2-IMP-H samples acquired during heating of the samples in the NH_3+O_2 mixture. (NH_3:O_2 ratio of 1:40, total pressure p_Σ~1.4 mbar).

the interaction with the reaction products and intermediates (H_2O, OH_{ads}). Also, a slight variation of the Pt4f line width during sample treatment in NH_3+O_2 mixture can be observed. The broadening of the Pt4f spectra was caused by the non-uniform charging of the particles surface during the *in situ* NAP-XPS experiments. See ESI for the details.

In case of the Pt/TiO_2-IMP-H sample the shift of the $Pt4f_{7/2}$ peak corresponding to the reduced Pt species is more noticeable. Some authors have shown that the encapsulation of the platinum particles by a support with the formation of TiO_x suboxide layer on the surface of the platinum particles can lead to a positive shift of $E_b(Pt4f_{7/2})$.[85,86] The encapsulation of the platinum particles by $TiO_{2-\delta}$ when heated in oxygen containing atmosphere is usually observed at rather high temperatures (T>400°C).[67,81] In our work lower temperatures were used, and the Pt4f/Ti2p intensity ratio changed insignificantly during heating of the sample in the reaction medium. Based on this, we believe that the encapsulation of the platinum particles by TiO_x suboxide should be excluded. Moreover, encapsulated Pt^0 particles are usually considered catalytically inactive,[44] while we did not observe decrease of the NH_3 conversion during heating. Similar to the Pt/TiO_2-IMP sample, we can assume that the shift of the Pt4f line can be either associated with the slight change of the surface conductivity during the reaction or with the formation of adsorbed oxygen species (O_{ad} and/or OH_{ad}) on the Pt^0 surface or within the Pt^0-TiO_2 boundary.

Thus, the NAP-XPS data do not show the formation of strongly oxidized platinum species (PtO_x layers or PtO/PtO_2

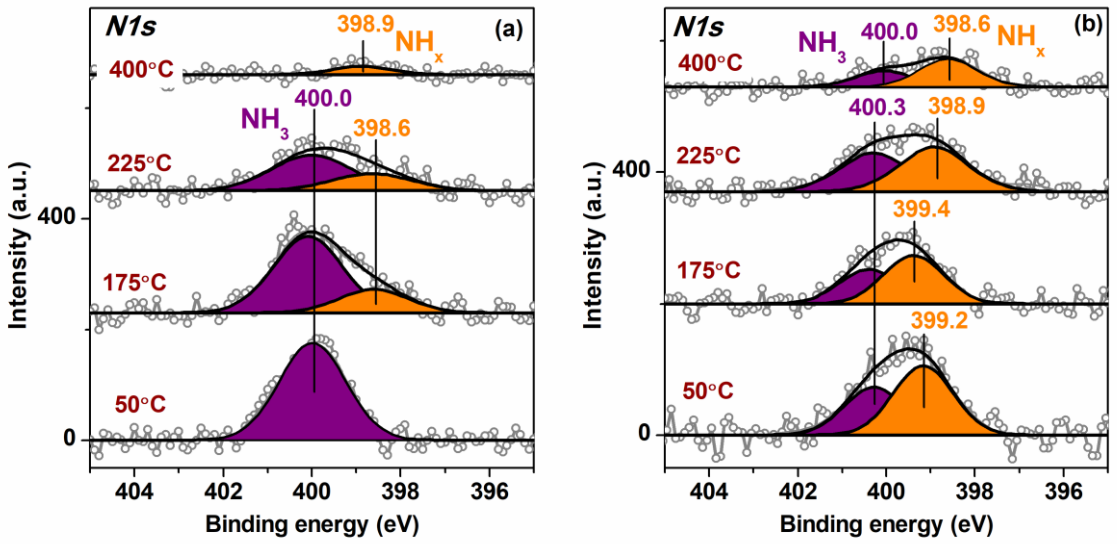

Fig.8. Curve-fitted *in situ* N1s XP spectra of (a) Pt/TiO_2-IMP and (b) Pt/TiO_2-IMP-H samples acquired during heating of the samples in the NH_3+O_2 mixture (NH_3:O_2 ratio of 1:40, total pressure p_t~1.4 mbar).

oxides) during NH_3 oxidation. The obtained data are in a good agreement with the results of the *in situ* study of the interaction of the bulk platinum surface with NH_3+O_2 reaction mixture,[10] pointing to similarity of the active sites.

Fig.8 presents *in situ* N1s spectra fitted to the individual components collected for the Pt/TiO_2-IMP (Fig.8a) and the Pt/TiO_2-IMP-H (Fig.8b) samples heated in the NH_3+O_2 mixture at different temperatures. The N1s spectra of the Pt/TiO_2-IMP sample treated in the NH_3+O_2 mixture at 50°C show the main peak with E_b(N1s)~400.0 eV. Such E_b value was observed after treatment of the TiO_2 support in NH_3 flow at 600°C.[87] The authors assign this N1s peak to Ti-O-N bond. Since we use much lower temperatures, doping of the TiO_2 surface under such conditions is unlikely. NH_3 species adsorbed on the surface of metallic Pt are also characterized by E_b(N1s)~400.0 eV.[8,10,88] Adsorption of NH_3 on the TiO_2 support surface should also take place. The increase of the temperature results in the appearance of the peak at 398.6-398.9 eV corresponding to adsorbed NH_x (x=1,2) forms.[8,88] The appearance of such forms indicates dehydrogenation of the NH_3 species, which is a first step of the NH_3 oxidation reaction.[11,89]

It should be noted that for the sample heated in the NH_3+Ar mixture the N1s spectra also show the peak of the adsorbed NH_3 species (E_b(N1s)~399.9-400.2 eV), as well as a peak with E_b(N1s)~398.2-398.4 eV, corresponding to the NH_{xad} (x=1,2) species (see ESI, Fig.S6). However, the impact of the adsorbed NH_x on the overall N1s spectrum at all temperatures is low. This result is in a good agreement with the literature data. It is known that the presence of oxygen species adsorbed on the surface of Pt^0 enhances dissociation of NH_3.[8,89]

At temperatures above 225°C the amount of the adsorbed NH_3 and NH_x decreases (Fig. 8). In the same temperature range, the selectivity of the reaction changes towards the formation of NO_x (Fig.S4). Desorption of NH_{xad} provides free sites for the oxygen adsorption thus causing a shift of the selectivity towards NO_x formation.[8] For the reduced Pt/TiO_2-IMP-H sample, the formation of the adsorbed NH_x is observed already at 50°C, and the contribution of these species to the overall N1s spectra is higher compared to the Pt/TiO_2-IMP sample in the entire temperature range. This may be related to the large number of platinum metal species that provide sites for adsorption of ammonia and oxygen. The predominant presence of the dehydrogenated NH_{xad} species rather than NH_{3ad} on the surface was reported for bulk metal Pt treated in NH_3+O_2 mixture.[10,90] Note that no NO_{ad} species were detected on the samples surface in a good agreement with literature data.[10] The NO desorption is considered to be much faster process than NO formation. It cannot be excluded that at the partial pressure used in NAP-XPS experiments the amount of the NO_x species adsorbed on the surface is not sufficient for the detection.

Fig.9 shows variation of the fraction of Pt^0 species for Pt/TiO_2-IMP and Pt/TiO_2-IMP-H samples during heating in the NH_3+O_2 mixture. The fraction of Pt^0 species was calculated as a ratio of the area of the Pt4f peak with E_b($Pt4f_{7/2}$)=70.8-71.4 eV

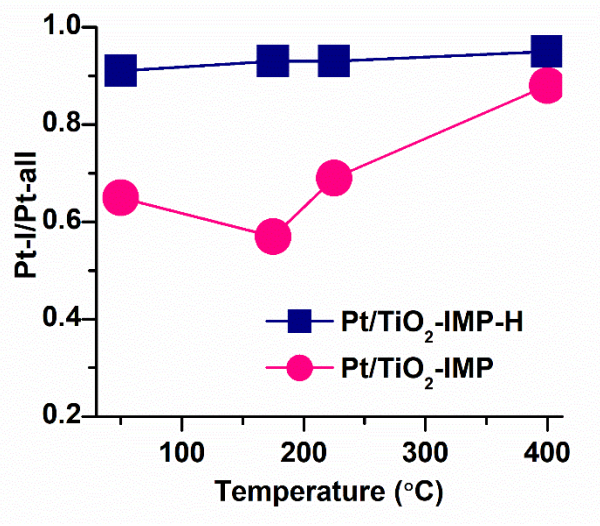

Fig.9. Variation of the fraction of the Pt4f peak with $E_b(Pt4f_{7/2})$=70.8-71.4 eV (Pt-I) to the overall Pt4f signal intensity for Pt-TiO_2-IMP and Pt-TiO_2-IMP-H samples during NAP-XPS study in the NH_3+O_2 mixture.

to the overall area of Pt4f spectrum. (Further, "Pt-I" stands for the Pt4f peak with $E_b(Pt4f_{7/2})$=70.8-71.4 eV). For the Pt/TiO_2-IMP sample, the fraction of the Pt-I peak decreases slightly with an increase of the reaction temperature from 50°C to 175°C, but increases at higher temperatures. The study of the thermal stability of the Pt/TiO_2-IMP sample (see ESI, Fig.S7) shows that PtO structures are not stable at temperature higher than 175°C, in a good agreement with literature data.[60,81,82] However, the contribution of the Pt^{4+} signal to the Pt4f spectrum remains practically unchanged up to 200°C (Fig.S7). We can propose that in O_2 flow the highly dispersed Pt sites remain in the Pt^{4+} state. The higher stability of PtO_x is known for smaller Pt particles.[62] Also, heating of the Pt/TiO_2-IMP sample in the reaction mixture from 50 to 225°C results in a slight increase of the Pt4f/Ti2p intensity ratio (from 0.07 to 0.1). The variation of the fraction of the Pt-I peak together with the change in the Pt4f/Ti2p intensity ratio points to the transition of the oxidized PtO to the Pt^0 sites with the adsorbed oxygen species at a temperature range up to 225°C. Such transition might be accompanied by the change of the sample morphology which results in the increase of the Pt4f/Ti2p intensity ratio. Temperature increase to 400°C leads to a significant increase of the fraction of the Pt-I peak as a result of the reduction of PtO and PtO_2 species and increase of the number of Pt^0 sites with the adsorbed oxygen species on the surface. A slight decrease of the Pt4f/Ti2p ratio at this temperature range (from 0.1 to 0.07) might indicate sintering of the platinum particles under treatment in the reaction mixture at higher temperatures. TEM data for the Pt/TiO_2-IMP sample after the reaction confirms a slight increase of the average size of the platinum particles (See ESI, Fig.S8). For the reduced Pt/TiO_2-IMP-H sample the fraction of the Pt-I peak remains practically unchanged with the temperature increase. No significant oxidation of the metal Pt^0 is taking place. Only

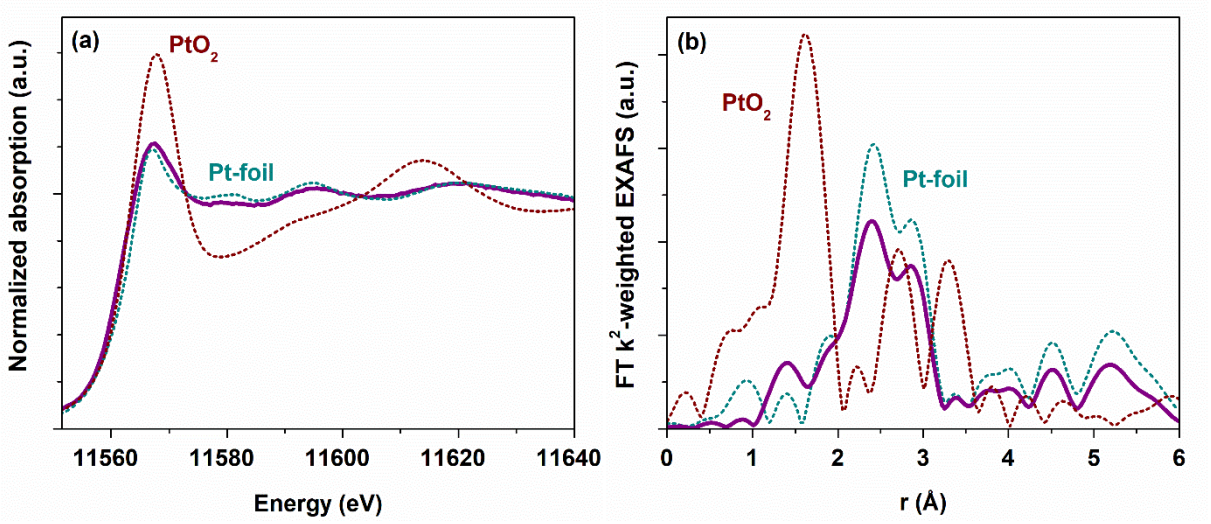

Fig.10. (a) *Ex situ* Pt L_3-XANES and (b) FT k^2-weighted EXAFS spectra of Pt/TiO_2-LAL sample (alongside the data for PtO_2 and metallic Pt reference samples). The EXAFS is Fourier-transformed in the k-range of: 2.5-11.0 $Å^{-1}$ and is not corrected for the phase shift.

oxygen species (O_{ad} and/or OH_{ad}) adsorbed on the Pt^0 surface are formed with the increase of the reaction temperature.

Thus, the NAP-XPS data show that the states of Pt in the analyzed samples upon their treatment in the NH_3+O_2 mixture at T>225°C are very similar and best described by Pt^0 surface. One can conclude that, despite the difference in the charge states of Pt in the as-prepared samples, the "active" states of the surface observed during the treatment of the samples in the NH_3+O_2 mixture are similar. The oxidized Pt species initially present in the Pt/TiO_2-IMP sample decompose with the temperature increase providing the metallic platinum sites available for oxygen adsorption.

XANES/EXAFS study of the Pt/TiO_2 samples

To follow the change of the platinum charge state during the reaction in the bulk, XANES and EXAFS spectroscopy were employed. The experiments were performed for the most active of the studied samples - Pt/TiO_2-LAL.

XANES and Fourier transformed (FT) extended X-ray absorption fine structure (EXAFS) spectra collected *ex situ* for the Pt/TiO_2-LAL sample are given in Fig.10. In a good agreement with the data of other methods, the sample contains mostly platinum in the metallic state. The average oxidation state determined by linear combination analysis (LCA) of the XANES data in the energy range between 11550 and 11600 eV is 0.6±0.1. These results are in a good agreement with the XPS data from which the average oxidation state can be estimated as 0.8. Somewhat lower oxidation state observed by XANES may be due to unaccounted number of large Pt NPs (see Fig.2b). FT k^2-weighted EXAFS spectra (Fig.10b) and the corresponding analysis (Table 2) reveal features very similar to metallic Pt with slightly lower intensity implying rather large (> 2 nm) Pt nanoparticles.[91] No Ti neighbor in the second shell was required to fit the experimental data. (k^2-weighted EXAFS functions and EXAFS fits for all analyzed samples are given in ESI, Fig.S9, and S10). So, EXAFS data do not clearly show the interaction of Pt particles with TiO_2 support (due to very low fraction of Pt atoms at the Pt-TiO_2 interface which would be invisible in the averaged signal). However, the Pt-TiO_2 interaction at the contact of the platinum particles with a TiO_2 surface cannot be ruled out.

Fig.11a presents a trend of the average oxidation state of platinum in the Pt/TiO_2-LAL sample during the heating in the NH_3+O_2 mixture (derived from LCA of *operando* XANES (see Fig.S11)), as well as the change of the NH_3 conversion and the yield of reaction products. According to the *operando* XANES analysis, the oxidation state of platinum does not change significantly during the catalytic reaction.

Fig.11b shows Fourier transformed extended X-ray absorption fine structure (EXAFS) spectra for the Pt/TiO_2-LAL

Table 2. Results of EXAFS fitting of Pt/TiO_2-LAL spectra to a structural model containing O and Pt nearest neighbors.

Experiment	Pt-O		Pt-Pt		DW factor (10^{-3} Å^2)	δE_0 (eV)	ρ (%)
	R (Å)	CN	R (Å)	CN			
ex situ	1.96±0.03	0.9±0.2	2.76±0.01	9.9±1.4	4.7±1.0	6.2±1.2	0.7
in situ (50°C)	2.03±0.05	0.9±0.5	2.76±0.02	11.1±3.3	6.2±2.2	7.8±2.2	1.6
in situ (400°C)	1.98±0.04	1.5±0.5	2.75±0.01	12.3±3.1	12.1±2.7	6.1±1.7	2.5
in situ (50°C), after heating-cooling cycle	2.04±0.07	1.1±0.8	2.76±0.02	10.2±4.6	5.5±3.2	8.5±3.7	2.9

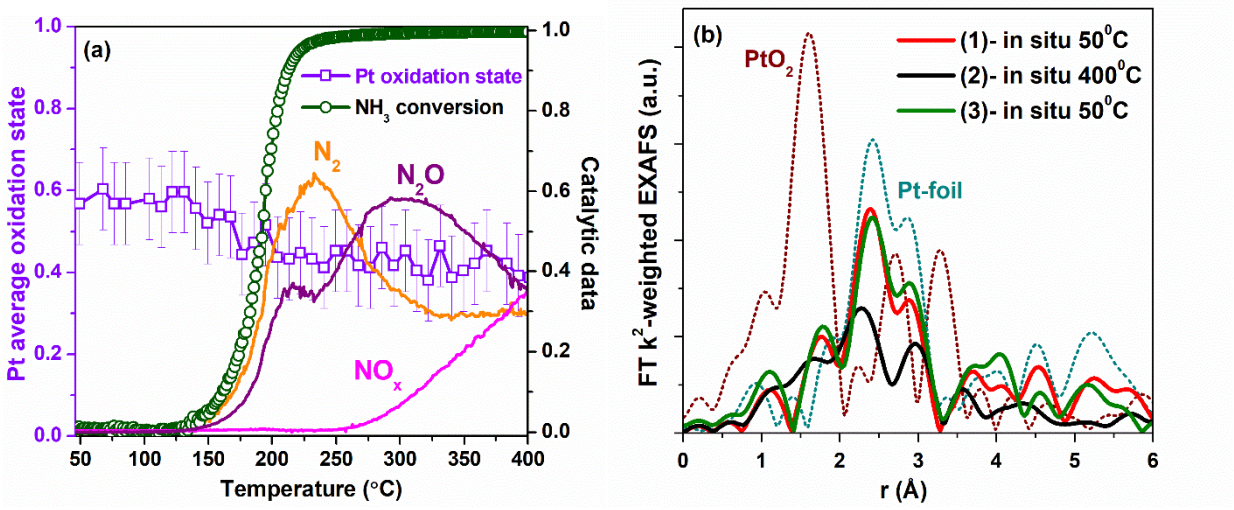

Fig.11. (a) NH_3 conversion, N_2, N_2O, and NO_x yields, and Pt average oxidation state profiles obtained from *operando* XANES experiments during heating of Pt/TiO_2-LAL in the NH_3+O_2 mixture. (The reaction mixture: 880 ppm NH_3, 10 vol.% O_2, and 10 vol.% N_2 in He). (b) FT k^2-weighted EXAFS spectra of Pt/TiO_2-LAL sample in NH_3 oxidation feed at (1) 50°C and (2) 400°C, and (3) after cooling down to 50°C. The EXAFS is Fourier-transformed in the k-range of: 2.5-11.0 Å^{-1} and is not corrected for the phase shift.

sample at temperature plateaus during NH_3 oxidation (during heating- at 50°C and 400°C, after cooling down in reaction mixture to 50°C). Platinum nanoparticles are rather stable during the experiment. The observed decrease in the backscattering intensity in the spectrum measured at 400°C can be attributed only to the increased disorder due to thermal motion (Debye-Waller factor). Qualitatively, one may notice an increased backscattering on the second Pt shell (3.5 – 4.5 Å) which may indicate sintering of Pt nanoparticles due to thermal cycling. Quantification of this effect by EXAFS is not possible due to limited data quality resulting in no statistically significant changes.

Thus, *in situ*/*operando* methods applied in our study allowed us to follow the evolution of Pt oxidation states under catalytic conditions. The use of NAP-XPS technique revealed the preservation of metallic Pt species on the surface of TiO_2

under NH_3+O_2 conditions even at high reaction temperatures (Fig.7). To bridge pressure gap between NAP-XPS experiments and realistic catalytic conditions *operando* XANES/EXAFS method was applied. Similar to the results of surface sensitive NAP-XPS, analysis of the average oxidation state of Pt within the bulk of the sample by *operando* XANES/EXAFS does not reveal significant oxidation of the metallic platinum species during the reaction, while the appearance of the oxygen species adsorbed on platinum surface cannot be excluded.

Previously, we performed *operando* XANES study of the Pt/Al_2O_3 samples in the NH_3+O_2 reaction.[69] In contrast to the Pt/TiO_2 system, it was shown that during the reaction at least 40% of the platinum surface remains oxidized in the form of the PtO_x layer regardless of the charge state of platinum in the initial Pt/Al_2O_3 catalysts.[69] We can propose that metal-support interaction in Pt/TiO_2 samples that is practically absent in case of Al_2O_3 support might influence the charge state of platinum and its reducibility.

Comparison of the results collected for Pt/TiO_2 samples prepared by different preparation techniques allowed us to conclude that for the stabilization of the catalytically active metallic Pt species through the metal-support interaction several approaches can be applied: a) the use of defective TiO_2 as a support that can be provided by application of the pulsed laser ablation in liquids; or b) the reductive pretreatment of highly dispersed Pt nanoparticles prepared by impregnation. *In situ*/*operando* methods revealed that, in contrast to Pt/Al_2O_3 samples,[69] thus stabilized metallic Pt state remains preserved during the reaction. The obtained results show that Pt/TiO_2 has a high potential for the catalytic application in ASC system as a catalyst for efficient ammonia oxidation at low temperatures.

Conclusions

The Pt/TiO_2 samples with different sizes of Pt particles and oxidation state of platinum were prepared by LAL and impregnation methods and tested as catalysts for the ammonia oxidation reaction. The catalysts containing metallic platinum particles showed activity at a lower temperature (T_{50}~150°C) than the catalysts initially containing oxidized platinum species (T_{50}~180°C). A combination of NAP-XPS and *operando* XAS methods was applied to follow the changes on the surface of the samples and within their bulk during the NH_3+O_2 reaction. NAP-XPS experiments allowed to differentiate the oxidation states of Pt on the surfaces and follow their evolution under the reaction conditions, as well as detect the surface intermediates. The results showed that decomposition of the PtO_x species with the formation of the metallic sites is required to initiate the NH_3+O_2 reaction. Only metallic Pt species were observed during the reaction without the formation of a stable PtO_x surface oxide layer. Based on the analysis of N1s spectra the NH_{3ads} and NH_{xads} species were detected on the samples surface during the NH_3+O_2 exposure. *Operando* XAS experiments allowed to analyze the sample under more realistic conditions at a higher partial pressure of the reagents. They unraveled that, similar to NAP-XPS results, the average oxidation state of Pt did not change significantly during the reaction with the metallic platinum being the main Pt state. Combination of *operando* XAS and NAP-XPS methods allowed to address the "pressure" gap problem. Similarity of the NAP-XPS and *operando* XAS results confirms the applicability of the NAP-XPS method for the analysis of the processes taking place on the samples surface during the catalytic reaction.

The NAP-XPS experiments were performed for the first time for the supported Pt catalysts in NH_3+O_2 reaction. The obtained results demonstrate a good correlation to the data obtained earlier during *in situ* XPS studies of ammonia oxidation over the model Pt systems (single crystals and foils). Thus, we address the "material" gap problem known for the model catalytic studies and confirm the relevance of the results collected on the model catalytic systems for the analysis of the powder catalysts.

A comparison with the results obtained previously for the Pt/Al_2O_3 catalysts suggests that the higher activity of the Pt/TiO_2 systems at lower temperatures might be associated with the metal-support interaction providing the stabilization of Pt in a metallic state. Thus, Pt/TiO_2 system should be further studied in details as a potential catalyst for low-temperature NH_3 oxidation.

Conflicts of interest

There are no conflicts to declare.

Acknowledgements

The work was supported by Helmholtz – Russian Science Foundation Joint Research Groups grant #18-43-06201 from 03.09.2018 (RSF)/HRSF-0046 from 01.09.2018 (HGF). We acknowledge the CERIC-ERIC Consortium for the access to near ambient pressure XPS facilities at Charles University; DESY (Hamburg, Germany), a member of the Helmholtz Association HGF, for the provided beamtime at PETRA III for *operando* XANES/EXAFS experiments; the resource center "VTAN" (Novosibirsk State University, Russia) for the access to the TEM equipment. We would like to thank Dr. Edmund Welter for assistance in using beamline P65 at DESY. We further thank Dr. Paolo Dolcet (KIT) for his support during the XAS measurements.

References

1 M. V. Twigg, *Appl. Catal. B Environ.*, 2007, **70**, 2–15.
2 P. L. Silveston and W. S. Epling, in *Periodic Operation of Chemical Reactors*, Elsevier Inc., 2013, pp. 141–170.
3 T. Johnson, *SAE Int. J. Engines*, 2013, **6**, 699–715.
4 O. Deutschmann and J.-D. Grunwaldt, *Chem. Ing.Techn.*, 2013, **85**, 595–617.
5 M. Colombo, I. Nova, E. Tronconi, V. Schmeißer, B. Bandl-Konrad and L. Zimmermann, *Appl. Catal. B Environ.*, 2013, **142**–**143**, 861–876.
6 S. Shrestha, M. P. Harold, K. Kamasamudram and A. Yezerets, *Catal. Today*, 2014, **231**, 105–115.

7 J. L. Gland and V. N. Korchak, *J. Catal.*, 1978, **53**, 9–23.
8 C. J. Weststrate, J. W. Bakker, E. D. L. Rienks, C. P. Vinod, A. V. Matveev, V. V. Gorodetskii and B. E. Nieuwenhuys, *J. Catal.*, 2006, **242**, 184–194.
9 J. Pérez-Ramírez, E. V. Kondratenko, V. A. Kondratenko and M. Baerns, *J. Catal.*, 2004, **227**, 90–100.
10 S. Günther, A. Scheibe, H. Bluhm, M. Haevecker, E. Kleimenov, A. Knop-Gericke, R. Schlögl and R. Imbihl, *J. Phys. Chem. C*, 2008, **112**, 15382–15393.
11 R. Imbihl, A. Scheibe, Y. F. Zeng, S. Günther, R. Kraehnert, V. A. Kondratenko, M. Baerns, W. K. Offermans, A. P. J. Jansen and R. A. Van Santen, *Phys. Chem. Chem. Phys.*, 2007, **9**, 3522–3540.
12 Y. Yao and K. P. Giapis, *Phys. Chem. Chem. Phys.*, 2016, **18**, 29858–29863.
13 J. J. Ostermaier, J. R. Katzer and W. H. Manogue, *J. Catal.*, 1974, **33**, 457–473.
14 M. Sun, S. Wang, Y. Li, H. Xu and Y. Chen, *Appl. Surf. Sci.*, 2017, **402**, 323–329.
15 M. Sun, J. Liu, C. Song, Y. Ogata, H. Rao, X. Zhao, H. Xu and Y. Chen, *ACS Appl. Mater. Interfaces*, 2019, **11**, 23102–23111.
16 J. Schäffer, V. A. Kondratenko, N. Steinfeldt, M. Sebek and E. V Kondratenko, *J. Catal.*, 2013, **301**, 210–216.
17 G. Olofsson, L. R. Wallenberg and A. Andersson, *J. Catal.*, 2005, **230**, 1–13.
18 Y. Li and J. N. Armor, *Appl. Catal. B Environ.*, 1997, **13**, 131–139.
19 J. J. Ostermaier, J. R. Katzer and W. H. Manogue, *J. Catal.*, 1976, **41**, 277–292.
20 M. Jabłońska, *Catal. Commun.*, 2015, **70**, 66–71.
21 D. A. Daramola and G. G. Botte, *Comput. Theor. Chem.*, 2012, **989**, 7–17.
22 M. Rafti, J. Luis, A. Albesa, A. Scheibe and R. Imbihl, *Surf. Sci.*, 2012, **606**, 12–20.
23 G. Novell-Leruth, A. Valcárcel, A. Clotet, J. M. Ricart and J. Pérez-Ramírez, *J. Phys. Chem. B*, 2005, **109**, 18061–18069.
24 H. Ma and W. F. Schneider, *J. Catal.*, 2020, **383**, 322–330.
25 J. D. Gonzalez, K. Shojaee, B. S. Haynes and A. Montoya, *Phys. Chem. Chem. Phys.*, 2018, **20**, 25314–25323.
26 E. V. Rebrov, M. H. J. M. De Croon and J. C. Schouten, *Chem. Eng. J.*, 2002, **90**, 61–76.
27 R. Kraehnert and M. Baerns, *Chem. Eng. J.*, 2008, **137**, 361–375.
28 A. Scheuer, M. Votsmeier, A. Schuler, J. Gieshoff, A. Drochner and H. Vogel, *Top. Catal.*, 2009, **52**, 1847–1851.
29 US Pat., US8524185B2, 2013.
30 T. Lan, Y. Zhao, J. Deng, J. Zhang, L. Shi and D. Zhang, *Catal. Sci. Technol.*, 2020, 5792–5810.
31 H. Huang, D. Y. C. Leung and D. Ye, *J. Mater. Chem.*, 2011, **21**, 9647–9652.
32 A. Lewera, L. Timperman, A. Roguska and N. Alonso-Vante, *J. Phys. Chem. C*, 2011, **115**, 20153–20159.
33 L. Y. Lin, S. Kavadiya, X. He, W. N. Wang, B. B. Karakocak, Y. C. Lin, M. Y. Berezin and P. Biswas, *Chem. Eng. J.*, 2020, **389**, 123450.
34 Z. Rui, L. Chen, H. Chen and H. Ji, *Ind. Eng. Chem. Res.*, 2014, **53**, 15879–15888.
35 Y. Zhou, D. E. Doronkin, M. Chen, S. Wei and J.-D. Grunwaldt, *ACS Catal.*, 2016, **6**, 7799–7809.
36 B. Imelik, C. Naccache, G. Coudurier, H. Praliaud, P. Meriaudeau, P. Gallezot, G. A. Martin and J. C. Vedrine, Eds., in *Studies in Surface Science and Catalysis*, 1982, pp. 1–384.
37 D. P. Sobczyk, E. J. M. Hensen, A. M. De Jong and R. A. Van Santen, *Top. Catal.*, 2003, **23**, 109–117.
38 E. M. Slavinskaya, T. Y. Kardash, O. A. Stonkus, R. V. Gulyaev, I. N. Lapin, V. A. Svetlichnyi and A. I. Boronin, *Catal. Sci. Technol.*, 2016, **6**, 6650–6666.
39 E. M. Slavinskaya, A. I. Stadnichenko, V. V. Muravyov, T. Y. Kardash, E. A. Derevyannikova, V. I. Zaikovskii, O. A. Stonkus, I. N. Lapin, V. A. Svetlichnyi and A. I. Boronin, *ChemCatChem*, 2018, **10**, 2232–2247.
40 E. Ogel, M. Casapu, D. E. Doronkin, R. Popescu, H. Störmer, C. Mechler, G. Marzun, S. Barcikowski, M. Türk and J.-D. Grunwaldt, *J. Phys. Chem. C*, 2019, **123**, 5433–5446.
41 E. D. Fakhrutdinova, A. V. Shabalina, M. A. Gerasimova, A. L. Nemoykina, O. V. Vodyankina and V. A. Svetlichnyi, *Materials*, 2020, **13**, 4–7.
42 G. L. Haller and D. E. Resasco, *Adv. Catal.*, 1989, **36**, 173–235.
43 K. Fujiwara, K. Okuyama and S. E. Pratsinis, *Environ. Sci. Nano*, 2017, **4**, 2076–2092.
44 X. Y. Shi, W. Zhang, C. Zhang, W. T. Zheng, H. Chen and J. G. Qi, *J. Microsc.*, 2016, **262**, 203–215.
45 E. A. Fedorova, A. I. Stadnichenko, E. M. Slavinskaya, L. S. Kibis, O. A. Stonkus, D. A. Svintsitskiy, I. N. Lapin, A. V. Romanenko, V. A. Svetlichnyi and A. I. Boronin, *J. Struct. Chem.*, 2020, **61**, 316–329.
46 Bruker, *TOPAS, Version 4.2*, Bruker AXS Inc., Madison, WI, USA, 2009.
47 M. D. Abramoff, P. J. Magalhaes and S. J. Ram, *Biophotonics Int.*, 2004, **11**, 36–42.
48 B. Ravel and M. Newville, *J. Synchrotron Radiat.*, 2005, **12**, 537–541.
49 M. Horn, C. F. Schwebdtfeger and E. P. Meagher, *Zeitschrift für Krist. - Cryst. Mater.*, 1972, **136**, 273–281.
50 P. Ballirano and R. Caminiti, *J. Appl. Crystallogr.*, 2001, **34**, 757–762.
51 M. Peuckert and H. P. Bonzel, *Surf. Sci.*, 1984, **145**, 239–259.
52 K. Vijay Kumar, *Zeitschrift fur Phys. Chemie*, 1991, **173**, 105–113.
53 A. V. Kalinkin, M. Y. Smirnov, A. I. Nizovskii and V. I. Bukhtiyarov, *J. Electron Spectros. Relat. Phenomena*, 2010, **177**, 15–18.
54 S. J. Tauster, S. C. Fung and R. L. Garten, *J. Am. Chem. Soc.*, 1978, **100**, 170–175.
55 T. Ioannides and X. E. Verykios, *J. Catal.*, 1996, **161**, 560–569.
56 Q. Fu and T. Wagner, *Surf. Sci. Rep.*, 2007, **62**, 431–498.
57 C. J. Pan, M. C. Tsai, W. N. Su, J. Rick, N. G. Akalework, A. K. Agegnehu, S. Y. Cheng and B. J. Hwang, *J. Taiwan Inst. Chem. Eng.*, 2017, **74**, 154–186.
58 J. Ohyama, A. Yamamoto, K. Teramura, T. Shishido and T. Tanaka, *ACS Catal.*, 2011, **1**, 187–192.
59 L. Nie, P. Zhou, J. Yu and M. Jaroniec, *J. Mol. Catal. A Chem.*, 2014, **390**, 7–13.
60 D. A. Svintsitskiy, L. S. Kibis, A. I. Stadnichenko, S. V. Koscheev, V. I. Zaikovskii and A. I. Boronin, *ChemPhysChem*, 2015, **16**, 3318–3324.
61 D. A. Svintsitskiy, E. M. Slavinskaya, O. A. Stonkus, A. V. Romanenko, A. I. Stadnichenko, L. S. Kibis, E. A. Derevyannikova, A. A. Evtushkova and A. I. Boronin, *J. Struct. Chem.*, 2019, **60**, 919–931.
62 A. Y. Stakheev, D. A. Bokarev, I. P. Prosvirin and V. I. Bukhtiyarov, in *Advanced Nanomaterials for Catalysis and Energy*, Elsevier, 2019, pp. 295–320.
63 A. Naitabdi, R. Fagiewicz, A. Boucly, G. Olivieri, F. Bournel, H. Tissot, Y. Xu, R. Benbalagh, M. G. Silly, F. Sirotti, J. J. Gallet and F. Rochet, *Top. Catal.*, 2016, **59**, 550–563.
64 A. Boubnov, S. Dahl, E. Johnson, A. P. Molina, S. B. Simonsen, F. M. Cano, S. Helveg, L. J. Lemus-Yegres and J.-D. Grunwaldt, *Appl. Catal. B Environ.*, 2012, **126**, 315–325.
65 A. M. Gänzler, M. Casapu, P. Vernoux, S. Loridant, F. J. Cadete Santos Aires, T. Epicier, B. Betz, R. Hoyer and J.-D. Grunwaldt, *Angew. Chemie Int. Ed.*, 2017, **56**, 13078–13082.
66 C. Wang and C. Yeh, *J. Catal.*, 1998, **178**, 450–456.
67 M. Zhang, Z. Jin, Z. Zhang and H. Dang, *Appl. Surf. Sci.*, 2005, **250**, 29–34.

68 B. Bahrami, V. G. Komvokis, M. S. Ziebarth, O. S. Alexeev and M. D. Amiridis, *Appl. Catal. B, Environ.*, 2013, **130–131**, 25–35.
69 D. A. Svintsitskiy, L. S. Kibis, A. I. Stadnichenko, E. M. Slavinskaya, A. V. Romanenko, E. A. Fedorova, O. A. Stonkus, D. E. Doronkin, V. Marchuk, A. Zimina, M. Casapu, J.-D. Grunwaldt and A. I. Boronin, *ChemCatChem*, 2020, **12**, 867–880.
70 S. Hinokuma, H. Shimanoe, S. Matsuki, M. Kawano, Y. Kawabata and M. Machida, *Chem. Lett.*, 2015, **45**, 179–181.
71 J. G. Wang, W. X. Li, M. Borg, J. Gustafson, A. Mikkelsen, T. M. Pedersen, E. Lundgren, J. Weissenrieder, J. Klikovits, M. Schmid, B. Hammer and J. N. Andersen, *Phys. Rev. Lett.*, 2005, **95**, 256102.
72 E. I. Vovk, A. V. Kalinkin, M. Y. Smirnov, I. O. Klembovskii and V. I. Bukhtiyarov, *J. Phys. Chem. C*, 2017, **121**, 17297–17304.
73 D. J. Miller, H. Öberg, S. Kaya, H. Sanchez Casalongue, D. Friebel, T. Anniyev, H. Ogasawara, H. Bluhm, L. G. M. Pettersson and A. Nilsson, *Phys. Rev. Lett.*, 2011, **107**, 195502–195507.
74 C. R. Parkinson, M. Walker and C. F. McConville, *Surf. Sci.*, 2003, **545**, 19–33.
75 D. R. Butcher, M. E. Grass, Z. Zeng, F. Aksoy, H. Bluhm, W.-X. Li, B. S. Mun, G. A. Somorjai and Z. Liu, *J. Am. Chem. Soc.*, 2011, **133**, 20319–20325.
76 D. Miller, H. Sanchez Casalongue, H. Bluhm, H. Ogasawara, A. Nilsson and S. Kaya, *J. Am. Chem. Soc.*, 2014, **136**, 6340–6347.
77 C. Puglia, A. Nilsson, B. Hernnäs, O. Karis, P. Bennich and N. Mårtensson, *Surf. Sci.*, 1995, **342**, 119–133.
78 S. P. Devarajan, J. A. Hinojosa and J. F. Weaver, *Surf. Sci.*, 2008, **602**, 3116–3124.
79 Z. Zhu, F. Tao, F. Zheng, R. Chang, Y. Li, L. Heinke, Z. Liu, M. Salmeron and G. A. Somorjai, *Nano Lett.*, 2012, **12**, 1491–1497.
80 M. Y. Smirnov, A. V. Kalinkin and V. I. Bukhtiyarov, *J. Struct. Chem.*, 2007, **48**, 1053–1060.
81 L. K. Ono, B. Yuan, H. Heinrich and B. R. Cuenya, *J Phys Chem C*, 2010, **114**, 22119–22133.
82 L. K. Ono, J. R. Croy, H. Heinrich and B. R. Cuenya, *J. Phys. Chem. C*, 2011, **115**, 16856–16866.
83 Y. Xu, W. A. Shelton and W. F. Schneider, *J. Phys. Chem. A*, 2006, **110**, 5839–5846.
84 J. E. Drawdy, G. B. Hoflmd, S. D. Gardner and E. Yngvadottir, *Surf. Inter. Anal.*, 1990, **16**, 369–374.
85 F. Pesty, H.-P. Steinrück and T. E. Madey, *Surf. Sci.*, 1995, **339**, 83–95.
86 Y. M. Sun, D. N. Belton and J. M. White, *J. Phys. Chem.*, 1986, **90**, 5178–5182.
87 Y. Wang, C. Feng, M. Zhang, J. Yang and Z. Zhang, *Appl. Catal. B Environ.*, 2011, **104**, 268–274.
88 C. J. Weststrate, J. W. Bakker, E. D. L. Rienks, C. P. Vinod, S. Lizzit, L. Petaccia, A. Baraldi and B. E. Nieuwenhuys, *Surf. Sci.*, 2006, **600**, 1991–2001.
89 D. P. Sobczyk, A. M. De Jong, E. J. M. Hensen and R. A. Van Santen, *J. Catal.*, 2003, **219**, 156–166.
90 D. P. Sobczyk, J. Van Grondelle, P. C. Thüne, I. E. Kieft, A. M. De Jong and R. A. Van Santen, *J. Catal.*, 2004, **225**, 466–478.
91 A. Jentys, *Phys. Chem. Chem. Phys.*, 1999, **1**, 4059–4063.